Eur. Phys. J. C (2005)
Digital Object Identifier (DOI) 10.1140/epjc/s2005-02179-y

THE EUROPEAN PHYSICAL JOURNAL C

String and parton percolation

C. Pajares[a]

Departamento de Física de Partículas Elementais e Instituto Galego de Física de Altas Enerxías, Universidade de Santiago de Compostela, 15782 Santiago de Compostela, Spain

Received: 17 January 2005 /
Published online: 8 April 2005 –

Abstract. A brief review to string and parton percolation is presented. After a short introduction, the main consequences of percolation of color sources on the following observables in A–A collisions: J/ψ suppression, saturation of the multiplicity, dependence on the centrality of the transverse momentum fluctuations, Cronin effect and transverse momentum distributions, strength of the two and three body Bose–Einstein correlations and forward–backward multiplicity correlations, are presented. The behavior of all of them can be naturally explained by the clustering of color sources and the dependence of the fluctuations of the number of these clusters on the density.

PACS. 2 5.75.-q, 12.38.Mh, 24.85.+p

1 Introduction

What conditions are necessary in the pre-equilibrium stage to achieve deconfinement and perhaps subsequent quark–gluon plasma formation? This question of the occurrence of color deconfinement in nuclear collisions without assuming prior equilibration has been addressed on the basis of two closely related concepts, string or parton percolation [1,2] and parton saturation [3–5]. In this paper we will study the first subject.

Consider a flat two dimensional surface S (the transverse nuclear area), on which N small discs of radius r_0 (the transverse partonic or string size) are randomly distributed, allowing for overlapping. With increasing density $n \equiv N/\pi R^2$ (we take here $S = \pi R^2$), clusters of increasing size appear. The crucial feature is that this cluster formation shows critical behavior: in the limit $N \to \infty$ and $R \to \infty$ with n finite, the cluster size diverges at a certain critical density. The percolation threshold is given by

$$\eta_{\rm c} = \pi r_0^2 \frac{N}{\pi R^2}, \tag{1}$$

and its value, 1.13, is determined by numerical studies. For finite N and R, percolation sets in when the largest cluster spans the entire surface from the center to the edge. Because of overlap, a considerable fraction of the surface is still empty at the percolation point, in fact, at the threshold, only $1 - \exp(-\eta_{\rm c}) \simeq 2/3$ of the surface is covered by discs.

In high energy nuclear collision, the strings or partons originate from the nucleons within the colliding nuclei; therefore their distribution on the transverse area of the collision is highly non-uniform, with more nucleons and hence more strings or partons in the center than in the edge. In this case the value of $\eta_{\rm c}$ becomes higher [6].

[a] e-mail: pajares@fpaxp1.usc.es

2 Local parton percolation and J/ψ suppression

Hard probes, such as quarkonia, probe the medium locally, and thus test only if it has reached the percolation point and the resulting geometric deconfinement at their location. It is thus necessary to define a more local percolation criterion [7].

As we mentioned before, at the percolating critical density, 1/3 of the surface remains empty. Hence disc density in the percolating cluster must be greater than $(3/2)(\eta_{\rm c}/\pi r_0^2)$. In fact numerical studies show that percolation sets in when the density of partons in the largest cluster reaches the critical value $1.72/\pi r_0^2$, slightly larger than $(3/2)(1.13/\pi r_0^2)$. This result provides the required local test: if the parton density at a certain point in the transverse nuclear collision plane has reached this level, the medium there belongs to a percolating cluster and hence to a deconfined parton condensate. In Fig. 1 the percolation probability and its derivative as a function of η are shown.

Let us apply the above idea to J/ψ suppression in A–A collisions [8]. We denote by $n_{\rm s}(A)$ the density of nucleons in the largest cluster within the transverse plane and by $\mathrm{d}N_q(x,Q^2)/\mathrm{d}y$ the parton distribution functions. (At central rapidity $y = 0$, we have $x = k_{\rm T}/\sqrt{s}$, where $k_{\rm T}$ denotes the transverse momentum of the partons and thus

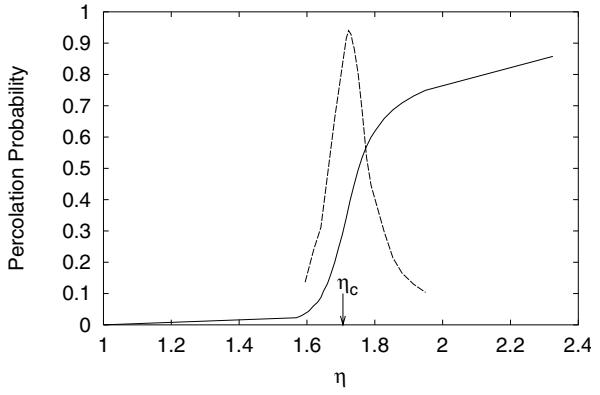

Fig. 1. Percolation probability and its derivative as a function of η

$k_{\mathrm{T}} \simeq Q$.) The local parton percolation condition is

$$n_{\mathrm{s}}(A)\left(\frac{\mathrm{d}N_q(x,Q_{\mathrm{c}}^2)}{\mathrm{d}y}\right)_{x=Q_{\mathrm{c}}/\sqrt{s}} = \frac{1.72}{\pi/Q_{\mathrm{c}}^2}. \qquad (2)$$

For a given A–A collision at a fixed centrality and energy, the relation (2) determines Q_{c}.

For Pb–Pb collisions at $\sqrt{s} = 17.4\,\mathrm{GeV}$, $Q_{\mathrm{c}} \simeq 0.7\,\mathrm{GeV}$. The scales of the charmonium states χ_{c} and ψ', as determined by the inverse of their radii calculated in potential theory, are around 0.6 GeV and 0.5 GeV respectively; therefore the parton condensate can thus resolve these states and all χ and ψ' states formed inside the percolating cluster disappear. The location is determined by the collision density. The first onset of J/ψ suppression in Pb–Pb collisions at SPS should occur at $N_{\mathrm{part}} \simeq 125$, where the $J/\psi's$ due to feed-down from χ_{c} and ψ' states in the percolating cluster are eliminated. Directly produced $J/\psi's$ survive because of their smaller radii (leading to a scales of 0.9–1.0 GeV) and its dissociation requires more central collisions, which lead to a better resolution, i.e. to an increase of Q_{c}. For $Q_{\mathrm{c}} = 1.0\,\mathrm{GeV}$ we need $N_{\mathrm{part}} \simeq 320$. The resolution scale of the direct J/ψ cannot be reached in S–U collisions; therefore only a one-step pattern suppression is obtained for this case.

For Au–Au collisions at RHIC, the increased parton density shifts the onset of percolation to a higher resolution scale, so that from the threshold on, all charmonium states including $J/\psi's$ are suppressed, starting at $N_{\mathrm{part}} \simeq 90$, i.e. a single-step suppression pattern occurs.

For the case of In–In collisions at SPS energies, the threshold for directly produced J/ψs is not reached even for the most central collisions, and again a single-step suppression pattern is expected.

A detailed discussion and comparison with experimental data can be found in [7, 9].

3 String percolation

Multiparticle production is currently described in terms of color strings stretched between partons of the projectile and target, which decay into new strings through q–$\bar{q}$ production and subsequently hadronize to produce observed hadrons. Color strings may be viewed as small discs in the transverse space, πr_0^2, $r_0 = 0.2$–$0.25\,\mathrm{fm}$, filled with the color field created by the colliding partons. Particles are produced by the Schwinger mechanism [10] emitting $q\bar{q}$ pairs in this field. With growing energy and/or atomic number of colliding particles, the number of strings grows and they start to overlap, forming clusters. At a critical density a macroscopic cluster appears that marks the percolation phase transition.

The percolation theory governs the geometrical pattern of the string clustering. Its observable implications, however, require the introduction of some dynamics to describe the string interaction, i.e., the behavior of a cluster formed by several overlapping strings.

It is assumed that a cluster behaves as a single string with a higher color field $\mathbf{Q_n}$ corresponding to the vectorial sum of the color charge of each individual $\mathbf{Q_1}$ string. The resulting color field covers the area S_n of the cluster. As $\mathbf{Q_n} = \sum_i^n \mathbf{Q_1}$, and the individual string colors may be oriented in an arbitrary manner respective to one another, the average $\mathbf{Q_{1i}Q_{1j}}$ is zero, and $\mathbf{Q_n}^2 = n\mathbf{Q_1}^2$.

Knowing the charge color $\vec{Q}_n$, one can compute the particle spectra produced by a single cluster of such color charge and area S_n using the Schwinger formula. For the multiplicity μ_n and average p_{T}^2 of particles, $\langle p_{\mathrm{T}}^2\rangle_n$, produced by a cluster of n strings one finds [11, 12]

$$\mu_n = \sqrt{n\frac{S_n}{S_1}}\mu_1, \quad , \quad \langle p_{\mathrm{T}}^2\rangle_n = \sqrt{\frac{nS_1}{S_n}}\langle p_{\mathrm{T}}^2\rangle_1, \qquad (3)$$

where μ_1 and $\langle p_{\mathrm{T}}^2\rangle_1$ are the mean multiplicity and mean p_{T}^2 of particles produced by a single string with a transverse area $S_1 = \pi r_0^2$. For strings just touching each other $S_n = nS_1$ and hence $\mu_n = n\mu_1, \langle p_{\mathrm{T}}^2\rangle_n = \langle p_{\mathrm{T}}^2\rangle_1$ as expected (simple fragmentation of n independent strings). In the opposite case of maximum overlapping, $S_n = S_1$ and therefore $\mu_n = \sqrt{n}\mu_1$, $\langle p_{\mathrm{T}}^2\rangle_n = \sqrt{n}\langle p_{\mathrm{T}}^2\rangle_1$, so that the multiplicity as a result is maximally suppressed. Notice that a certain conservation rule holds:

$$\frac{\mu_n}{n}\langle p_{\mathrm{T}}^2\rangle_n = \mu_1\langle p_{\mathrm{T}}^2\rangle_1, \qquad (4)$$

and also the scaling law

$$\langle p_{\mathrm{T}}^2\rangle_n/\mu_n S_n = \langle p_{\mathrm{T}}^2\rangle_1/\mu_1 S_1. \qquad (5)$$

In the limit of high density

$$\langle nS_1/S_n\rangle = \frac{\eta}{1-\exp(-\eta)} \equiv \frac{1}{F^2(\eta)},$$
$$\eta = N_S\pi r_0^2/\pi R^2. \qquad (6)$$

Thus

$$\mu = N_S F(\eta)\mu_1 \ ; \ \langle p_{\mathrm{T}}^2\rangle = \langle p_{\mathrm{T}}^2\rangle_1/F(\eta). \qquad (7)$$

The universal scaling law (5) is valid for all projectiles and targets, different energies and centralities, being in reasonable agreement with the experimental data [13]. A similar scaling is found in the color glass condensate approach [14].

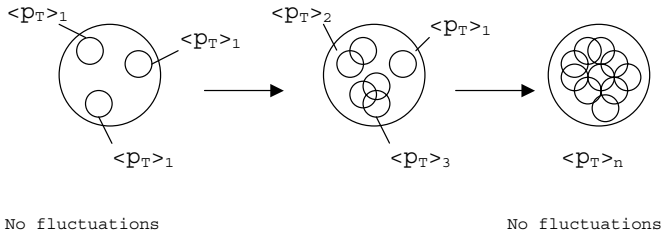

Fig. 2. Cluster formation for low, intermediate and high density respectively

Notice that $N_S \sim N_{\rm coll} \sim N_A^{4/3}$ at central rapidity (at the fragmentation region $N_S \sim N_{\rm part} \sim N_A$). As $F(\eta) \sim N_A^{1/3}$, $\mu \sim N_A$.

Therefore, the multiplicity per participant does not depend on the number of participants; there is saturation. Numerical studies show a good agreement with SPS and RHIC data [12]. The prediction for central Pb–Pb collisions ($N_A = 400$) at LHC ($\sqrt{s} = 5.5\,\text{GeV}$) is $\mu/0.5N_{\rm part} = 8.6$ and the total charged multiplicity per unit rapidity (at central rapidity) is 1800. These numbers are very similar to the ones obtained from Hera data, assuming scaling, using PQCD and the BK equation [16,17].

4 Transverse momentum fluctuations

The behavior of the transverse momentum fluctuations can be understood as follows: At low densities most of the particles are produced by individual strings with the same $\langle p_{\rm T}\rangle_1$, so the fluctuations must be small. Similarly, at large density, above the percolation critical point, there is essentially one cluster formed by almost all the strings created in the collision and therefore fluctuations are not expected either. Indeed, the fluctuations are expected to be maximal when the number of different clusters becomes larger, just below the percolation critical density (see Fig. 2). In this case in addition to the normal fluctuations around the mean transverse momentum of a single string, there are more fluctuations due to the different average transverse momentum of each cluster.

Experimentally, a measurement has been made of the quantity

$$F_{pt} \equiv \frac{\omega_{\rm Data} - \omega_{\rm random}}{\omega_{\rm random}}, \qquad \omega = \frac{\sqrt{\langle p_{\rm T}^2\rangle - \langle p_{\rm T}\rangle^2}}{\langle p_{\rm T}\rangle}, \quad (8)$$

where $\omega_{\rm random}$ denotes the corresponding normalized fluctuations in the case of statistically independent particle emission.

In Fig. 3 our result [18] compared with the experimental data is shown. A reasonable agreement is obtained. There is an alternative explanation based on the occurrence at RHIC of minijets which will enhance the $p_{\rm T}$ fluctuations. At high centrality, it is well established that the suppression of high $p_{\rm T}$ particles at RHIC can explain the suppression of fluctuations seen at lower centralities. According to this picture, at SPS where the production of minijets is negligible, this behavior is not expected, contrary to the expectations of percolation of strings.

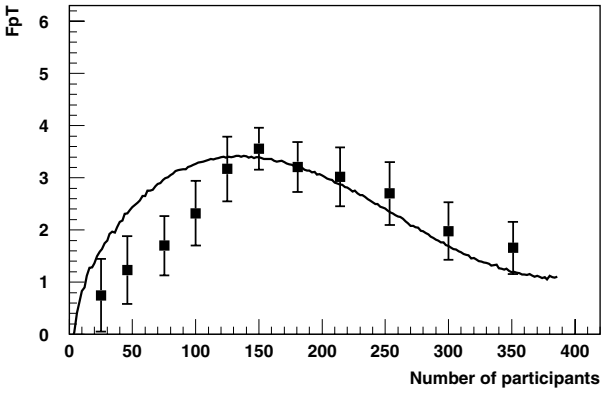

Fig. 3. $F_{p_{\rm T}}(0/0)$ versus the number of participants. Experimental data from PHENIX at $\sqrt{s} = 200\,\text{GeV}$. Solid line is for our results

Instead of $p_{\rm T}$ fluctuations, the NA49 Collaboration [19] have measured $(\langle n_-^2\rangle - \langle n_-\rangle^2)/\langle n_-\rangle$ at SPS for Pb–Pb collisions, as a function of the centrality of the collision, showing a maximum at low centrality and being 1 at high centrality. This behavior has nothing to do with minijets. On the contrary, it is explained naturally in our approach [20].

5 Universal transverse momentum distributions

In order to know the transverse momentum distributions one needs the fragmentation function $f(x, p_{\rm T})$ for each cluster, and the mean squared transverse momentum distribution of the clusters, $W(x)$, which is related to the cluster size distribution through (3). For $f(x, p_{\rm T})$ we assume the Schwinger formula, $f(x, p_{\rm T}) = \exp(-p_{\rm T}^2 x)$, used also for the fragmentation of a Lund string [21], at first approximation x is related to the string tension or equivalently to the inverse of the mean transverse momentum squared. For the weight function $W(x)$ we choose the gamma distribution

$$W(x) = \frac{\gamma}{\Gamma(k)}(\gamma x)^{k-1}\exp(-\gamma x). \quad (9)$$

The reason of this choice is the following: In peripheral heavy ion collisions there is almost no overlapping between the formed strings and therefore the cluster size distribution is peaked around low values. Most of the clusters are made of one single string. As the centrality increases the number of strings grows, so there are more and more ones overlapping among the strings, and the cluster size distribution is strongly modified, according to Fig. 4 where three cluster distributions corresponding to three different centralities of the collision are shown. Each curve in Fig. 4 can be reproduced by gamma distributions with different k values.

Moreover, the increase of centrality can be seen as a transformation of the cluster size distribution of the type

$$P(x) \to \frac{xP(x)}{\langle x\rangle} \to \ldots \to \frac{x^k P(x)}{\langle x^k\rangle} \to \ldots. \quad (10)$$

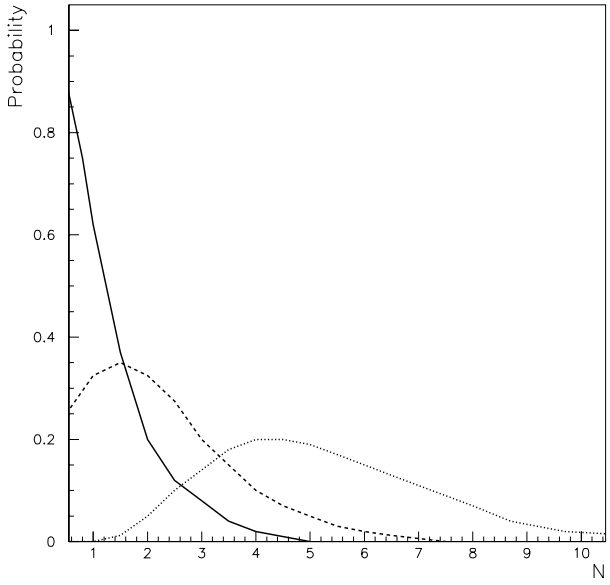

Fig. 4. Schematic representation of the number of clusters as a function of the number of strings of each cluster at three different centralities (the solid line corresponds to the most peripheral one and the pointed line to the most central one)

This kind of transformation were studied long time ago by Jona-Lasinio in connection to the renormalization group in probabilistic theory [22]. Actually an increase of the centralities is equivalent to a transformation which changes cells (single strings) by blocks (clusters) and the corresponding variables μ_1 and $\langle p_{\rm T}^2\rangle_1$ of the cells by μ_n and $\langle p_{\rm T}^2\rangle_n$. These transformations of the type of the chain (10) have been used also to study the probability associated to events which satisfy some requirements [23].

The γ and k parameters of the gamma distribution are related to the mean x and dispersion of the distribution through

$$\langle x\rangle = \frac{k}{\gamma}, \qquad \frac{\langle x^2\rangle - \langle x\rangle^2}{\langle x\rangle^2} = \frac{1}{k}. \tag{11}$$

We use (7) to take into account the effect of overlapping of strings, and hence $f(x, m_{\rm T}) = \exp(-p_{\rm T}^2 x F(\eta))$. Therefore we obtain

$$\frac{1}{\left(1+\frac{F(\eta)p_{\rm T}^2}{k\langle p_{\rm T}^2\rangle_1}\right)^k} = \int_0^\infty {\rm d}x\, \exp(-p_{\rm T}^2 x F(\eta))\frac{\gamma}{\Gamma(k)}(\gamma x)^{k-1}\exp(-\gamma x), \tag{12}$$

and the normalized $p_{\rm T}$ distribution is

$$f(p_{\rm T}, y) = \frac{{\rm d}N}{{\rm d}y}\frac{(k-1)F(\eta)}{k\langle p_{\rm T}^2\rangle_1}\frac{1}{\left(1+\frac{F(\eta)p_{\rm T}^2}{k\langle p_{\rm T}^2\rangle_1}\right)^k}. \tag{13}$$

Equation (12) can be seen as a superposition of chaotic color sources (clusters) where $1/k$ fixes the transverse momentum fluctuations. At small density $\eta << 1$, the strings are isolated and there are no fluctuations, $k \to \infty$. When the density increases, there will be some overlapping of strings forming clusters; the fluctuations increase and k decreases. The minimum of k will be reached when the fluctuations in the number of strings per cluster reach its maximum. Above this point, increasing η, these fluctuations decrease and k increases. In the limit, when only one cluster of all strings is formed, there are no fluctuations and again $k \to \infty$.

The obtained power-like behavior $(p_{\rm T}^2)^{-k}$, with an exponent k related to some intrinsic fluctuations, is common to many apparently different systems, as sociological, biological or informatic ones. Distributions like the citations of scientific works, or other complex networks [25, 26] where the probability $P(m)$ of having a given node with m links is described by the free scale power law $P(m) \sim (m)^{-k}$ with k related to the fluctuations in the number of links obey the same behavior. Also, it has been shown [27, 28] that maximization of the non-extensive information Tsallis entropy leads to the same distribution (12).

This universal behavior indicates the importance of the common features present in those phenomena, namely, the cluster structure and the fluctuations in the number of objets per cluster.

From (13) one can calculate

$$\frac{{\rm d}\ln f}{{\rm d}\ln p_{\rm T}} = \frac{-2F(\eta)}{\left(1+\frac{F(\eta)}{k}\frac{p_{\rm T}^2}{\langle p_{\rm T}^2\rangle_i}\right)}\frac{\langle p_{\rm T}^2\rangle}{\langle p_{\rm T}^2\rangle_{1i}}, \tag{14}$$

where "i" refers to the different particle species.

As $p_{\rm T}^2 \to 0$ this reduces to $-2F(\eta)p_{\rm T}^2/\langle p_{\rm T}^2\rangle_i$.

This behavior has been confirmed by the PHOBOS Collaboration. As $\langle p_{\rm T}^2\rangle_{1p} \geq \langle p_{\rm T}^2\rangle_{1k} \geq \langle p_{\rm T}^2\rangle_{1\pi}$ the absolute value is larger for pions than for kaons and than for protons.

Now, let us discuss the interplay between low and high $p_{\rm T}$. One defines the ration $R_{CP}(p_{\rm T})$ between central and peripheral collisions as

$$R_{CP}(p_{\rm T}) = \frac{f'(p_{\rm T}, y=0)/N'_{\rm coll}}{f(p_{\rm T}, y=0)/N_{\rm coll}}, \tag{15}$$

where the distribution in the numerator corresponds to higher densities $\eta' > \eta$. In the $p_{\rm T} \to 0$ limit, taking into account that $\frac{2}{3} \leq \frac{k-1}{k} \leq 1$ and that $F(\eta') < F(\eta)$, we obtain

$$R_{CP}(0) \simeq \left(\frac{F(\eta')}{F(\eta)}\right)^2 < 1, \tag{16}$$

approximately independent of k and k'. As η'/η increases, the ratio $R_{CP}(0)$ decreases, in agreement with the experimental data.

As $p_{\rm T}$ increases we have

$$R_{CP}(p_{\rm T}) \sim \frac{1+F(\eta)p_{\rm T}^2/\langle p_{\rm T}^2\rangle_{1i}}{1+F(\eta')p_{\rm T}^2/\langle p_{\rm T}^2\rangle_{1i}}, \tag{17}$$

and $R_{CP}(p_{\rm T})$ increases with $p_{\rm T}$ (again, $F(\eta) > F(\eta')$).

At large $p_{\rm T}$,

$$R_{CP}(p_{\rm T}) \sim \frac{F(\eta)}{F(\eta')}\frac{k'}{k}(p_{\rm T}^2)^{k-k'}, \tag{18}$$

which means that if we are in the low density regime $k > k'$ and $R_{CP}(p_{\rm T}) > 1$, and we reproduce the Cronin effect. As we increase the energy, the density increases and one reaches the high density regime where $k' < k$ and suppression of $p_{\rm T}$ occurs. The Cronin effect disappears at high energies and/or densities. The critical density at which the Cronin effect disappears is the same at which the transverse momentum fluctuations presents a maximum.

$R_{CP}(p_{\rm T})$ for two different particles, for instance p and π, becomes, at intermediate $p_{\rm T}$,

$$\frac{R^p_{CP}(p_{\rm T})}{R^\pi_{CP}(p_{\rm T})} \simeq \left(\frac{\langle p^2_{\rm T}\rangle_{1p}}{\langle p^2_{\rm T}\rangle_{1\pi}}\right)^{k'-k}. \qquad (19)$$

As $\langle p^2_{\rm T}\rangle_{1p} > \langle p^2_{\rm T}\rangle_{1\pi}$, in the high density limit (Au–Au collisions with $k' > k$) we expect a ratio larger than 1, as the experimental data show.

As far as we approach the low density limit, the ratio decreases, becoming closer to 1 or even lower.

A more detailed comparison with experimental data on Au–Au, d–Au collisions with discussion of the forward rapidity region can be found in [24]. An overall reasonable agreement is obtained. It is very remarkable that such an agreement is based on the universal behavior of the $p_{\rm T}$ distribution given by (13).

6 Bose–Einstein correlations

Most of the studies of two body Bose–Einstein (B–E) correlations have paid attention to the parameters $R_{\rm side}$, $R_{\rm out}$, $R_{\rm L}$ and not to the strength of the correlation, defined by the chaoticity parameter

$$C_2(0,0) = \lambda. \qquad (20)$$

Experimentally, due to Coulomb interference and to the necessary extrapolations there are many uncertainties in its evaluation; however, some trend of the dependence of λ on the multiplicity can be established. First, SPS minimum bias data for O–C, O–Cu, O–Ag and O–Au collisions show that λ decreases as the size of the target increases, from $\lambda = 0.92$ up to $\lambda = 0.16$. However for S–Pb and Pb–Pb central collisions, where the values of η are larger, λ is also larger: $\lambda \simeq 0.5$–0.7.

This behavior can easily be explained in the percolation framework [29]. Each cluster can be considered as a chaotic source, $\lambda = 1$, and the production of particles from several clusters can be seen as the superposition of chaotic sources. In this scheme, $\lambda = n_{\rm s}/n$, being $n_{\rm s}$ the number of pairs produced in the same cluster and $n_{\rm T}$ the total number of pairs. In this way, λ is proportional to the inverse of the number of independent sources (clusters); therefore it decreases with the density up to the critical percolation value. From this critical value, it increases with density. This behavior is shown in Fig. 5.

Similar considerations can be done concerning the strength of the three body B–E correlations, ω. The NA44 Collaboration have obtained for S–Pb collisions $\omega = 0.20 \pm 0.02 \pm 0.19$ and for central Pb–Pb collisions

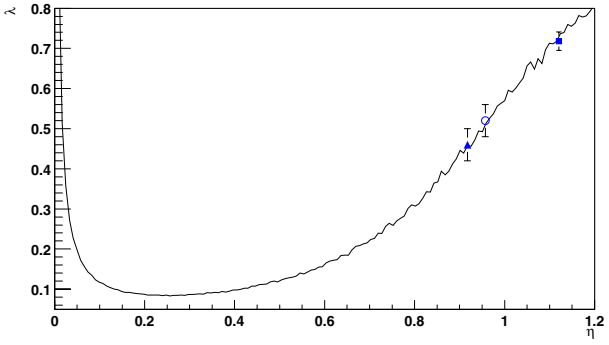

Fig. 5. λ as a function of η. Experimental points are for semicentral S–Pb collisions (filled triangle), 18% central Pb–Pb collisions (non-filled circle) and 10% central Pb–Pb collisions (filled box) at SPS

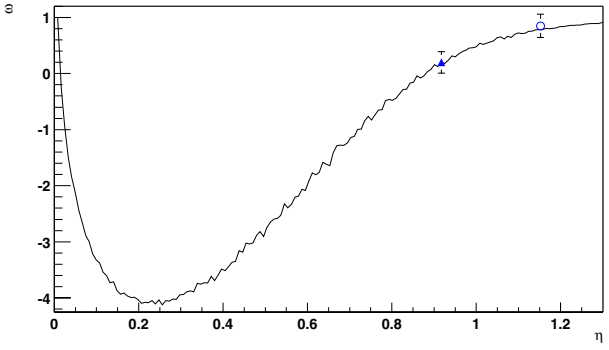

Fig. 6. ω as a function of η. Experimental points are for S–Pb semicentral collisions and 9% central Pb–Pb collisions at SPS

$\omega = 0.85 \pm 0.02 \pm 0.21$. The STAR Collaboration obtain for central Au–Au collisions values of ω close to 1. This sharp variation from $\omega = 0.2$ to $\omega = 0.8$–1 in a small range of η is easily explained in the framework of percolation of strings. Now ω becomes proportional to the inverse of the squared of the number of independent sources (clusters) which can accommodate a stronger variation compared to the case of two bodies. In Fig. 6 our result is shown [30].

7 Forward–backward correlations

A useful observable to check the percolation approach is the forward–backward correlation measured by the quantity

$$D_{\rm FW} = \langle n_{\rm F} n_{\rm B}\rangle - \langle n_{\rm F}\rangle\langle n_{\rm B}\rangle, \qquad (21)$$

where $n_{\rm F(B)}$ denotes the multiplicity in a forward (backward) rapidity interval. In order to eliminate the short range correlations, the forward and backward intervals should be separated by at least one unit of rapidity. On general grounds, one can see that $D_{\rm FW}$ is proportional to the fluctuations on the number of independent sources (or clusters in our case) [31, 32]. At very low density, $D_{\rm FW}$ should be very small, increasing with the density up to a maximum related to the largest number of clusters. At very high density, there are essentially only clusters and hence $D_{\rm FW}$ becomes small again.

There are some experimental data measuring the parameter b, through

$$\langle \mu_{\rm B} \rangle_{\rm F} = a + b\mu_{\rm F}, \tag{22}$$

where $b \equiv D_{\rm FB}/D_{\rm FF}$. The data on pp and pA show an increase of b with energy and density. Our prediction for high density is that b will decrease. Measurements of $D_{\rm FW}$ or b as a function of centrality would be welcome.

8 Conclusion

The percolation of partons and strings can correctly describe several observables, namely J/ψ suppression, multiplicities, transverse momentum fluctuations, transverse momentum distributions and B–E correlations. The behavior of all of them has a common physical basis: the clustering of color sources and the dependence of the number of clusters on the density. In this way, the threshold of J/ψ suppression, the maximum of transverse momentum fluctuations, the suppression of the Cronin effect and the turnover of the dependence of the strength of two and three body correlation with the energy are related to each other and all of them point out a percolation phase transition. Another test of this transition is the measurements of forward–backward correlations and also the multiplicity distributions not discussed here [33].

Many of the results obtained in the framework of percolation of strings are very similar to the one obtained in the color glass condensate (CGC). In particular, very similar scaling laws are obtained for the product and the ratio of the multiplicities and transverse momentum. For this reason, it is very tempting to identify the momentum $Q_{\rm s}$ which established the scale in CGC with the corresponding one in percolation of string. In this way

$$Q_{\rm s}^2 = \frac{k\langle p_{\rm T}^2 \rangle_1}{F(\eta)}. \tag{23}$$

The consequences of (23) are under study.

Acknowledgements. I thank the organizers for such a nice meeting and E.G. Ferreiro for a critical reading of the manuscript. This work has been done under contracts FPA2002-01161 of CICyT of Spain, and PGIDIT03PXIC-20612PN from Galicia.

References

1. N. Armesto, M.A. Braun, E.G. Ferreiro, C. Pajares, Phys. Rev. Lett. **77**, 3736 (1996)
2. M. Nardi, H. Satz, Phys. Lett. B **442**, 14 (1998)
3. L.V. Gribov, E.M. Levin, M.G. Ryskin, Phys. Rep. **100**, 1 (1983); J.P. Blaizot, A.H. Mueller, Nucl. Phys. B **289**, 847 (1987)
4. L.D. McLerran, R. Venugopalan, Phys. Rev. D **49**, 2233 (1994); D **49**, 3352 (1994); D **50**, 2225 (1994)
5. E. Iancu, A. Leonidov, L.D. McLerran, Nucl. Phys. A **692**, 583 (2001);
   E.G. Ferreiro, E. Iancu, A. Leonidov, L.D. McLerran, Nucl. Phys. A **710**, 5414 (2002)
6. A. Rodrigues, R. Ugoccioni, J. Dias de Deus, Phys. Lett. B **458**, 402 (1999)
7. S. Digal, S. Fortunato, H. Satz, Eur. Phys. J. C **32**, 547 (2004); S. Digal, S. Fortunato, P. Petrezky, H. Satz, Phys. Lett. B **549**, 547 (2004)
8. S. Digal, P. Petreczky, H. Satz, Phys. Rev. D **64**, 094015 (2001); T. Matsui, H. Satz, Phys. Lett. B **178**, 416 (1986)
9. M. Nardi, this volume
10. J. Schwinger, Phys. Rev. D **82**, 664 (1951); T.S. Biro, H.B. Nielsen, J. Knoll, Nucl. Phys. B **245**, 449 (1984)
11. M.A. Braun, C. Pajares, Eur. Phys. J. C **16**, 349 (2000)
12. M.A. Braun, F. del Moral, C. Pajares, Phys. Rev. C **65**, 024907 (2002)
13. J. Dias de Deus, E.G. Ferreiro, C. Pajares, R. Ugoccioni, Phys. Lett. B **581**, 156 (2004)
14. L.D. McLerran, J. Schaffner-Bielich, Phys. Lett. B **514**, 29 (2001); J. Schaffer-Bielich, D. Kharzeev, L.D. McLerran, R. Venugopalan, Nucl. Phys. A **705**, 494 (2002)
15. J. Dias de Deus, R. Ugoccioni, A. Rodrigues, Eur. Phys. J. C **16**, 537 (2000); J. Dias de Deus, R. Ugoccioni, Phys. Lett. B **494**, 53 (2000); **491**, 253 (2000)
16. N. Armesto, C.A. Salgado, U.A. Wiedemann, hep-ph/0407018
17. D. Kharzeev, M. Nardi, Phys. Lett. B **507**, 121 (2001); D. Kharzeev, E. Levin, M. Nardi, hep-ph/0408050
18. E.G. Ferreiro, F. del Moral, C. Pajares, Phys. Rev. C **69**, 034901 (2004); J. Dias de Deus, A. Rodrigues, hep-ph/030811
19. NA49 Collaboration, M. Rybczynski et al., nucl-ex/0409009
20. J. Dias de Deus, this volume
21. B. Andersson, The Lund model (Cambridge Univ. Press 1998)
22. G. Jona-Lasinio, Nuovo Cimento B **26**, 99 (1975)
23. J. Dias de Deus, C. Pajares, C.A. Salgado, Phys. Lett. B **408**, 417 (1997); B **407**, 335 (1997); B **409**, 474 (1997); J. Dias de Deus, C. Pajares, Phys. Lett. B **442**, 395 (1998)
24. J. Dias de Deus, E.G. Ferreiro, C. Pajares, R. Ugoccioni, hep-ph/030400, submitted to Eur. Phys. J. C
25. G. Koh, G. Laurent, Science **284**, 96 (1999)
26. R. Albert, A.L. Barabasi, Rev. Mod. Phys. **74**, 47 (2002)
27. G. Wilk, Z. Wlodarczyk, Acta Phys. Pol. B **35**, 2141 (2004); Phys. Rev. Lett. **84**, 2770 (2000)
28. C. Tsallis, J. Statist. Phys. **52**, 479 (1988)
29. M.A. Braun, F. del Moral, C. Pajares, Eur. Phys. J. C **21**, 557 (2001)
30. M.A. Braun, F. del Moral, C. Pajares, Phys. Lett. B **551**, 291 (2003)
31. N.S. Amelin, N. Armesto, M.A. Braun, E.G. Ferreiro, C. Pajares, Phys. Rev. Lett. **73**, 2813 (1994)
32. M.A. Braun, C. Pajares, Phys. Rev. Lett. **85**, 4864 (2000); M.A. Braun, R.S. Kolevatov, C. Pajares, V.V. Vechernin, Eur. Phys. J. C **32**, 535 (2004)
33. J. Dias de Deus, E.G. Ferreiro, C. Pajares, R. Ugoccioni, Phys. Lett. B **601**, 125 (2004)
34. M.A. Braun, C. Pajares, Phys. Lett. B **603**, 21 (2004); C. Pajares, Acta. Phys. Pol. B **35**, 153 (2004)